AN APPROACH TO THE MODELING OF
3-DIMENSIONAL STRONG MOTIONS

by

H. Umemura[I], J. Penzien[II], Y. Ohsaki[I] and M. Watabe[III]

SUMMARY

The maximum values of accelerations, velocities and displacements of the earthquake records are first discussed utilizing the historical and instrumental data as well as some theoretical approaches. Then, duration time and deterministic intensity function of the accelerograms are introduced. The predominant periods and spectral shapes of the strong motion accelerograms are also reported. Finally, the concept of principal axes of the 3-dimensional accelerograms is demonstrated so that the simulation of 3-dimensional strong accelerograms may stochastically be possible in the very near future.

MAXIMUM VALUES OF GROUND MOTION

(1) Evaluation by overturning of the tombstones:

Fig.-1 illustrates the relation between the epicentral distance (km) and the maximum acceleration estimated by overturned tombstones, bases on the data of the earthquake with the magnitude greater that 7 since 1927 in Japan. According to this figure, the maximum acceleration may exceed the value of 0.4g and upper bound of the maximum acceleration at ground surface appears to be around 0.6g.

(2) Evaluation by the records of the strong motion seismographs:

The maximum accelerations measured by the strong motion accelerographs on the hard subsoil layers are tabulated in Table 1. In Fig.-2, the relation between the epicentral distances and the maximum velocity values measured by the strong motion seismographs are indicated with the parameter of the magnitude [1]. It may be noticed that the maximum velocity ever record by the seismographs is approximately 35 kines as may be observed by this Fig.-2.

(3) Estimation of upper bound from the critical strain level of the rocks: [2]

Assuming the critical maximum strain of the fracture of the rocks (ε_{cr}) as $\varepsilon_{cr}=10^{-4}$ and shear wave velocity in the rock (Vs) as Vs=3km/sec., the maximum velocity value is estimated as 30 kines by the following equation.

$$\mu(z,t)=f(t-\frac{z}{Vs}) \qquad \varepsilon=\left|\frac{\sigma\mu}{\sigma z}\right|_{max}=\left|\frac{\partial f}{\partial t}\frac{1}{Vs}\right|_{max}=\frac{V}{Vs} \leqq \varepsilon_{cr}$$

where μ: amplitude of seismic wave in terms of time t: time z: coordinate along the wave propagation Vs: shear wave velocity ε: strain

From the above estimation, it is suggested that there is little chance for the maximum velocity to exceed the value of 30 kines.

(4) Proposal by Prof. K. Kanai:

By his vast experiences on earthquake enigneering, he proposed the following equation for the relation between the hypocentral distance and the maximum velocity (V_{max}) with the parameter of the magniutde of the earthquake [3].

$$V_{max}=10^{0.61M-(1.66+\frac{3.6}{x})\log x\ -\ (0.631+\frac{1.83}{x})}$$

I Professor of University of Tokyo, Dept. of Architecture

II Professor of University of California, Berkeley, California

III Head of Earthquake Engineering, International Institute of Seismology & Earthquake Engineering, Building Research Institute

where V_{max}: the maximum velocity on the surface of the bed-rock (kine)
M: the magnitude of the earthquake x: the hypocentral distance (km)
While the radius (D Km) of the shperical volume within which hypocenters of after-shocks of the earthquake exist can be expressed in terms of the magnitude (M) followingly,

$$D(km) = 10^{0.353M - 1.134} \quad [4]$$

Assuming that the above value D is depth of the hypocenter and using the Kanai's equation of the maximum velocity the relation between the maximum velocity and the epicentral distance can be expressed as illustrated in Fig.-3 with the parameter of the magnitude. The intersection of the relevant magnitude line and the dotted line indicates the radius (D km) in the above equation or, let us say, the depth of the hypocenter. Fig.-3 suggests that the maximum probable velocity value will never exceed the value of 60 kines.

(5) The ratio of the maximum acceleration to the maximum velocity:

From the 75 sets of the strong motion accelerograms and the corresponding velocity records obtained in both Japan and the United States, the mean value of these ratios is 9.95 in horizontal components and the standard deviation of those ratios is 1.7, while in vertical component, the above accelerograms and the corresponding velocity records do not coincide in time domain, however, those maxima will be regarded as closely correlated if the above time difference of the peaks is limited within one second. Selecting such records, the mean value of the ratios of the maximum acceleration to the maximum velocity is 11.0 in horizontal components and the standard deviation of those ratios is 1.8. In vertical component, the mean value and the standard deviation of those ratios are 13.8 and 1.7, respectively. Incidentally, the mean value of the ratios of the maximum acceleration to the corresponding maximum displacement is 20.6 and the standard deviation of those ratios is 3.3 for horizontal components. In case of the vertical component, the mean value and the standard deviation of those ratios are 18.0 and 1.9, respectively. Using the same materials including vertical components as well, a stochastic analysis is also made on the cross-correlations between the maximum values of acceleration, velocity, displacement and Housner's spectral intensity with zero and 0.2 dampings. The results are indicated in Table 2 from which it may be suggested that measures to represent intensity of ground motions such as values mentioned above are extremely cross-correlated, therefore the choice of these measures is allowed to be rather arbitrary.

(6) The ratio of the maximum acceleration in vertical component to those in the corresponding horizontal components:

From the same sets of the strong motion accelerograms mentioned (5), those ratios are obtained. Fig. - 4 shows some of these results. It might be reasonable to associate the epicentral distance with those ratios of the vertical maximum accelerations to the horizontal ones. The results suggest that shorter the epicentral distance is, the larger this ratio becomes. This ratio of the maximum acceleration in vertical component to those in the corresponding horizontal components, $\overline{R}(d)$, can be approximated followingly by the results.

$$\overline{R}(d) = e^{-0.0022(\frac{x}{x_0} + 300)}$$

where x is the epicentral distance in kilometer and x_0 is unit distance of kilometer. In spite of the above results, this ratio of the maximum acceleration in vertical component to those in the corresponding two horizontal components follows the complete characteristics of Guassian random process as may be ovserved in Fig.-5, in which probability disrtibution of variables as logarithm of the above ratio is plotted in solid line with the reference plots (in dotted line) of true Gaussian distribution.

(7) Summary:

As for the maximum velocity value, Fig.-3 might be regarded as reasonable considering the results of critical maximum strain. However it is also the fact that the maximum velocity ever recorded is 35 kines as already introduced in Fig.-2 and the upper bound area in Fig.-3 is the results by the exterpolation of the value actually recorded. It is quite controversial to define the maximum acceleration value, however in stochastic sense, this value can represent a reasonable measure for intensity parameter. This may mean to exclude a single peak value of the acceleration with frequency higher than 20 Hz for the stochastically significant value. The values indicated in Table 3 can be regarded as the "mean value of the maximum", therefore, in actual cases, many of the maximum values may exceed the values in the table.

DURATION TIME AND DETERMINISTIC INTENSITY

From 76 accelerograms obtained by 56 strong motion earthquakes during the years between 1968 and 1971 in Japan, the duration time (t) of accelerograms determined by the engineering judgement can be expressed followingly in terms of the magnitude of the earthquake (M),

$$t=10^{\frac{M-2.5}{3.23}}(\text{sec.})$$

According to research work on length (L,km) and displacement (D,m) of the active faults, there are relations[5]

$$\log D=0.60M-3.91 \qquad \log L=0.60M-2.91 \quad R=D/s$$

where s: average displacement velocity (m/year) M: magnitude of caused earthquake R: period of earthquake occurrence (year). With the rapture velocity along the fault as 3 km/sec., total rapture duration of the earthquake can be calculated using the above relation. The results are also indicated in Fig.-6.

(2) Deterministic intensity function:

Figs.-7 are the results of efforts to find the deterministic intensity function from the actual accelerograms by smoothing technics of the oscillatory irregular waves. It is suggested by Figs.-7, that the deterministic intensity function of ideal model [6] and the generalization of this pattern is somewhat controversial, but desirable from engineering point of view. It should be also noted that the deterministic intensity functions for the vertical components are not identical to those for the horizontal components as may be seen in Figs.-7. Another approach to obtain the pattern of deterministic intensity function is carried out by J. Penzien and T. Kubo [7].

SPECTRAL AND PHASE CHARACTERISTICS

(1) Spectral shape of the accelerograms on the surface of the bed-rock:

The transfer function to transmit the seismic wave around the bed-rock layers might be regarded as uniform in frequency domain, i.e., the spectral shape of the transfer function is "White". The spectral shape of the accelerograms on the surface of the bed-rock may be subjected to the influence of the spectral shape of sour e mechanisms and the surroundings of the hypocenters. Fig.-8 shows the response spectra of the accelerograms obtained on the same surface of the bed-rock layer. In this figure, spectra denoted A, B and C are obtained from accelerograms with 5% of critical damping ratio actuated by the following different earthquakes at the same station;

(A) earthquake M=4.3 epicentral distance 48km B) earthquake M=5.5 epicentral distance 150km C) earthquake M=6.0 epicentral distance 145km

Fig.-8 suggests that there is little common spectral peak among three, except the minor peak at about the period of 0.11 sec. and o.3 sec., the spectral characteristics appear to be greatly influenced by the characteristics of the earthquake itself. Fig.-9 suggests the predominant period of the displacement records of the earthquake [1]. This figure is obtained from the displacement of the seismic waves. It may be noted that the predominant periods for acceleration and displacement are completely the other thing except the fact that the larger the magnitude of the earthquake, the longer the predominant period becomes.

(2) Phase characteristics:

The phase difference for every circular frequency is completely random. There seems to be no correlation among them. This fact may clearly be seen by Fig.-10.

CONCEPT OF PRINCIPAL AXES OF THE ACCELEROGRAMS

In this paper, only the outline of the concept of principal axes of ground motions are introduced. Details are explained in [8]. First, 3 components of accelerograms along three orthogonal coordinate axes be defined through the relations

$$a_x(t)=\zeta(t)\ b_x(t), \quad a_y(t)=\zeta(t)\ b_y(t), \quad a_z(t)=\zeta(t)\ b_z(t)$$

where $b_x(t)$, $b_y(t)$ and $b_z(t)$ are stationary random processes and $\zeta(t)$ is a deterministic intensity function giving appropriate non-stationarity to the ground motion process. If $a_x(t)$, $a_y(t)$ and $a_z(t)$ are considered to be zero-mean non-stationary random processes, the covariance functions

$$E[a_i(t)a_j(t+\tau)] = \zeta(t)\ \zeta(t+\tau)\ E[b_i(t)b_j(t+\tau)] \quad i,j=x,y,z$$

where E denotes ensemble average, can be used to characterize the ground motion process. Since random processes $b_x(t)$, $b_y(t)$ and $b_z(t)$ are stationary, all ensemble averages on the right side of the above equation are independent of time t; therefore, showing dependence only upon the time difference τ. Since real earthquake accelerograms demonstrate a very rapid loss in correlation with increasing values of $|\tau|$, the infulence of coordinate directions on the covariance functions can be investigated by considering the relations

$$E[a_i(t)a_j(t)] = \zeta(t)^2 E[b_i(t)b_j(t)] \quad i,j=x,y,z$$

Defining covariance matrix $\underline{\beta}$ as

$$\underline{\beta}= \begin{bmatrix} \beta_{xx} & \beta_{xy} & \beta_{xz} \\ \beta_{yx} & \beta_{yy} & \beta_{yz} \\ \beta_{zx} & \beta_{zy} & \beta_{zz} \end{bmatrix}$$

where $\beta_{ij}=E[b_i(t)b_j(t)]$, the total covariance matrix can be written in the form $\underline{\mu(t)}=\zeta(t)^2\ \underline{\beta}$. By coordinate transformation of $a_x(t)$, $a_y(t)$ and $a_z(t)$ into new set of accelerograms $a_1(t)$, $a_2(t)$ and $a_3(t)$ along new three orthogonal coordinate axes, covariance matrix can be transformed into diagonal elements only, that is, $\beta_{ij}=0$; $i\neq j$. Such new axes which satisfies the above conditions are defined as principal axes where no cross-term of covariance exist and 3 variances of diagonal elements become the maximum, minimum and intermediate. Using the defined orthogonal transformation, principal axes of ground motion have been located for six different earthquakes. Variances and covariences of the recorded accelerations $a_x(t)$, $a_y(t)$ and $a_z(t)$ along the three accelerograph axes x, y and z respectively, were obtained. By selecting successive intervals over the entire duration of motion, the changes in direction of principal axes with time can be checked. Fig.-11 shows the horizontal directions of one principal axis for the above mentioned six earthquakes using sufficiently long time intervals to reasonably stabilize the principal coordinate directions. The corresponding variances are indicated by arrow lengths applied to the radial scale. In most cases the principal axis shown in Fig.-11 is the major principal axis; however, in some cases, usually for intervals near the ends of the motions when intensities have decreased considerably, the major

principal axis is at right angles to the directions shown. The minor principal axis is in each case nearly vertical. When averaging over the entire duration of motion and averaging for the six earthquakes, the resulting ratios of intermediate and minor principal variances to the major principal variance are approximately 3/4 and 1/2, respectively, i.e. $(\mu_{11}/\mu_{22})_{avg} \doteq 3/4$ and $(\mu_{33}/\mu_{11}) \doteq 1/2$. Using these numerical values to obtain principal covariances, the principal cross-correlation coefficients become $\rho_{12}=(\mu_{11}-\mu_{22})/(\mu_{11}+\mu_{22})=0.14$, $\rho_{23}=(\mu_{22}-\mu_{33})/(\mu_{22}+\mu_{33})=0.20$ and $\rho_{13} \pm (\mu_{11}-\mu_{33})/(\mu_{11}+\mu_{33})=0.33$.
Finally it is suggested that the potential use of the concept of principal axes to explore physical phenomena, such as tracing the center of energy release, should be investigated.

BIBLIOGRAPHY

1. Watabe. M. and Kitagawa. Y., 1973, Characteristics of Strong Motion Earthquake Obtained in Japan, 5th U.J.N.R.
2. Muramatsu. I. etal., 1963, Observation of Micro-Earthquake in Mino District in Gifu Prefecture, General Japan Journal of Phys. of the Earth
3. Kanai. K., 1966, Improved Empirical Formula for Characteristics of Strong Earthquake Motions, Proc. Japan Earthquake Symposium, (in Japan), pp.1-4
4. Iida. K., 1963, A Relation of Earthquake Energy to Tsunami Energy and the Estimation of the Vertical Displacement in a Tsunami Source, Journal of Earth Science Nagoya Univ. vol. 11, pp.49-67
5. Matsuda. T., 1975, Magnitude and Recurrence Interval of Earthquakes from a Fault, Zishin Vol. 28, pp.269-283
6. Jennings, P.C., Housner. G.W. and Tsai. N.C., April 1969, Simulated Earthquake Motions Earthquake Engineering Research Laboratory, California Institute of Technology, Pasadena
7. Penzien. J. and Kubo. T., 1977, Characteristics of Three-Dimensional Ground Motions Along Principal Axes, San Fernando Earthquake, WCEE
8. Penzien. J. and Watabe. M., 1975, Simulation of 3-Dimensional Earthquake Ground Motions, International Journal of Earthquake Engineering, McGraw-Hill

Table 1 : Max. acceleration by strong motion accelerographs on hard subsoil

Earthquake	Date	M	Location	Epicentral Distance	Subsoil	Max. Acc. (gal)
Matsushiro	1966. 4.5	6.1	Hoshina A	8.0		550
	1966. 5.28	4.9	Matsushiro B	3.5		370
	1966. 8.8	-	Hoshina B			390
Tokachioki	1968. 5.16	7.9	Miyako	115	Hard	118
			Horomanbashi		"	69
Higashi-matsuyama	1968. 7.1	6.4	HibiyaDenden	50	Gravel	27
			Shintonebashi	32	Hard	75
			Sakaigawa-bashi	48	"	55
Hidaka-Sankei	1970. 1.21	6.7	Horomanbashi	20	Rock	182

Table 2 : Coherence among measures to represent the intensity of ground motions

	A	V	D	$SI_{0.0}$	$SI_{0.2}$
A	0.905	0.841	0.587	0.830	0.902
V	0.892	0.798	0.876	0.957	0.986
D	0.739	0.888	0.702	0.826	0.770
$SI_{0.0}$	0.815	0.923	0.786	0.924	0.970
$SI_{0.2}$	0.911	0.960	0.791	0.960	0.897

A half above the diagonal : Horizontal and horizontal
A half below the diagonal : Vertical and vertical
Diagonal matrix : Horizontal and vertical
A : Maximum acceleration V: Maximum velocity
D : Maximum displacement SI: Housner's intensity
(ξ ξ: damping ratio)

Table 3 : The mean maximum values

	Horizontal	Vertical (epicentral distance within 20km)
Max. acceleration (gals)	605	304.3
Max. velocity (kines)	55	22.1
Max. displacement (cm)	29.4	16.9

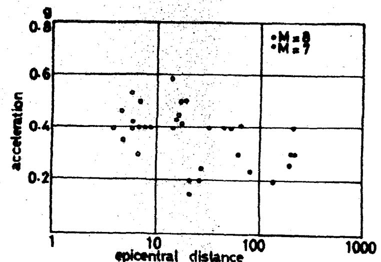

Fig.-1 Max. acceleration estimated by overturning of tombstones

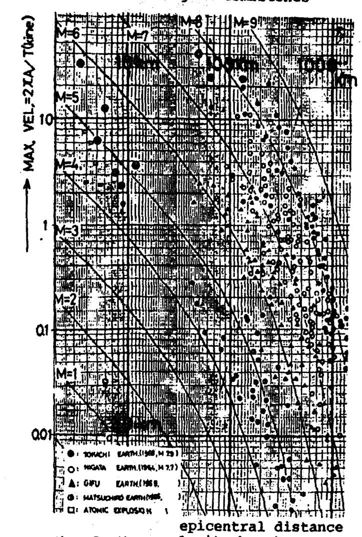

Fig.-2 Max. velocity by strong motion seismograph

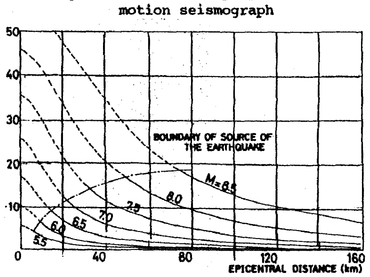

Fig.-3 Epicentral distance and Max. velocity

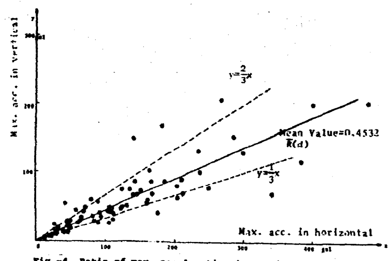

Fig.-4 Ratio of max. acceleration in vertical components to the one in horizontal components

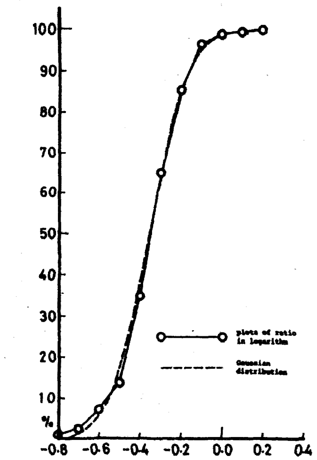
Fig.-5 Probability distribution plots of variables as logarithm of ratio (vertical VS. horizontal Housners intenisty with 20% damping)

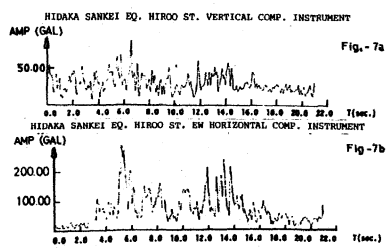

Fig.-7 Smoothed accelerograms to find the intensity deterministic function

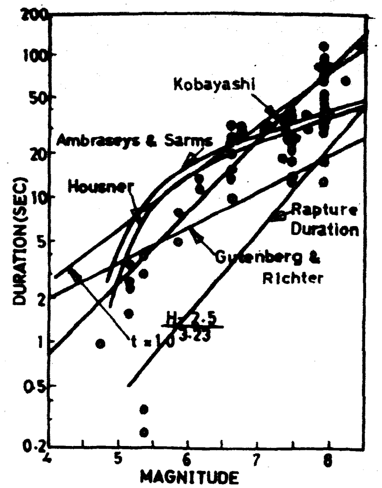

Fig.-6 Duration and magnitude proposed by various researchers

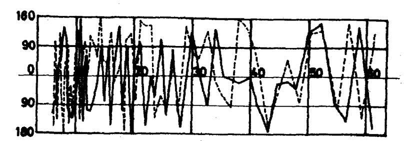
Fig.-10 Phase characteristics of accelerograms obtained at the same station

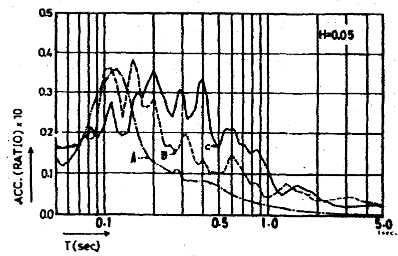

Fig.-8 Response spectra of the different earthquake obtained in the same station

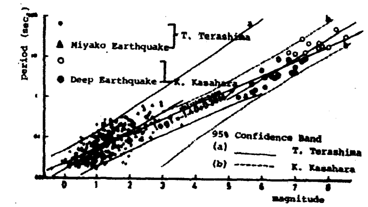

Fig.-9 Relation between magnitude and period

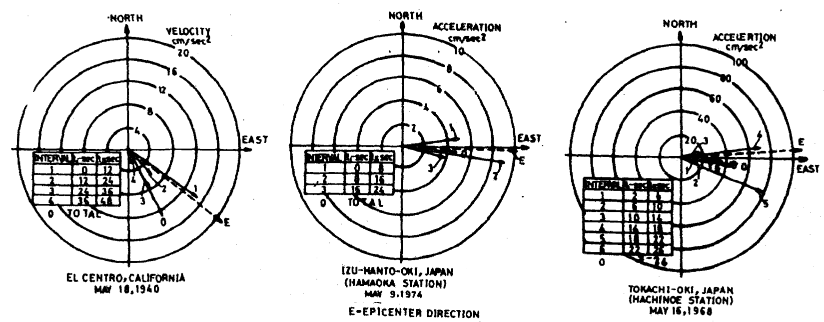

Fig.-11 Principal axis directions for 3 different recorded earthquake ground motions